Yields of neutron-rich nuclei by actinide photofission in the giant dipole resonance region

Debasis Bhowmick,* Debasis Atta,† D. N. Basu,‡ and Alok Chakrabarti§
Variable Energy Cyclotron Centre, 1/AF Bidhan Nagar, Kolkata 700 064, India
(Received 9 January 2015; revised manuscript received 20 March 2015; published 14 April 2015)

The photonuclear reactions of actinides induced by bremsstrahlung γs are studied in the region of nuclear excitation energies that covers the entire giant dipole resonance region. A comparative analysis of the behavior of the symmetric and asymmetric modes of photon-induced fission as a function of the average excitation energy of the fissioning nucleus is performed. The mass distributions for photofission fragments are obtained. The integrated yield as well as charge distribution of photofission products is determined. Thus, the production cross sections of neutron-rich nuclei are calculated and their exoticity (neutron richness) is explored in comparison to the nuclei produced by rapid neutron capture process in nucleosynthesis.

DOI: 10.1103/PhysRevC.91.044611 PACS number(s): 27.90.+b, 25.20.Dc, 25.85.Jg, 29.25.Rm

I. INTRODUCTION

Photonuclear reactions, along with neutron-induced fission, have been studied for several decades. New reliable studies on the mass distributions of fission fragments have become necessary in order to produce neutron-rich ion beams [1,2] (especially in the vicinity of ^{78}Ni) which, in turn, will open new vistas in the study of nuclei far away from the valley of stability. Moreover, the study of mass and charge distribution in low-energy photon- or neutron-induced fission of actinides will provide experimentalists an opportunity to study nuclear structures and dynamics of a wide range of fission products. The use of the energetic electrons is a promising tool to get intense neutron-rich ion beams. The Advanced Rare Isotope Laboratory (ARIEL) at TRI University Meson Facility (TRIUMF) is under construction [3], where a superconducting electron Linear Accelerator (LINAC) will produce 25-MeV, 100-kW e-beams for photofission (10^{13} fission/s) of uranium in the first phase. Yields of around 10^{11} fission/s of uranium by photofission have been experimentally achieved at Joint Institute of Nuclear Research (JINR), Dubna [4], and at Accélérateur Linéaire auprès du Tandem d'Orsay (ALTO), Institut de Physique Nucléaire (IPN), Orsay [5], by using 25-MeV, 20-μA e-beam. As an extension of the present RIB development, a facility called the Advanced National Facility for Unstable and Rare Isotope Beams (ANURIB) will be created at this center with e-LINAC as primary accelerator for photofission [6]. Therefore, photofission of uranium is a very powerful mechanism to produce such radioactive ion beams (RIB). Although the photofission cross section at giant dipole resonance (GDR) energy for ^{238}U is about an order of magnitude lower than for the 40-MeV neutron-induced fission, still it is advantageous because the electron and γ-photon conversion efficiency is much more significant than that for the deuterons and neutrons. Moreover, at lower energies the photofission and neutron-induced fission cross sections become comparable [7], making the latter further disadvantageous. For producing neutron-rich radioactive ion beam by the photofission method, nuclei are excited by photons covering the peak of the GDR where the energetic beam of incident electrons of $\sim$30 MeV can be stopped in a tungsten (W) converter or directly in the target uranium carbide (UC_2) itself, generating bremsstrahlung photons [8], which can induce fission.

In the present study, the total photoabsorption cross section at energies covering the GDR region are calculated while the mass distributions are analyzed on the basis of the multimode-fission model [9,10] and the charge distribution of photofission products are estimated. The mass distribution is interpreted as a sum of contributions of various fission modes: specifically, a symmetric mode (SM) and two asymmetric modes (ASMI and ASMII) associated with an enhanced yield of fission products. The average excitation energy for such a nucleus is used for the predictions of the multimode-fission model. A calculation of the contributions from various fission modes to the mass distribution of photofission fragments was performed in Ref. [11] at two accelerator energies. Without quantitative calculations, the existence of contributions from various fission modes was highlighted in Ref. [12]. In the present work, we perform a simultaneous analysis and a comparison of the behavior of the symmetric and asymmetric modes of photofission induced by bremsstrahlung photons in the region of excitation energies of the ^{238}U at the endpoint bremsstrahlung energy of 29.1 MeV, which corresponds to mean photon energy of 13.7 ± 0.3 MeV [13] that coincides with GDR peak for ^{238}U photofission. The results obtained in this way are compared with the predictions of the multimode-fission model for the dependence of individual fission modes on the excitation energy of the fissioning nucleus. The integrated yield of ^{238}U photofission and charge distribution of photofission products are calculated. The roles of photofission mass yield and its charge distribution in the production of neutron-rich nuclei are explored.

*dbhowmick@vecc.gov.in
†datta@vecc.gov.in
‡dnb@vecc.gov.in
§alok@vecc.gov.in

II. THE GDR PHOTOABSORPTION AND FISSION

In the hydrodynamic theoryof photonuclear reactions, the giant dipole resonance consists of a Lorentz line for spherical

TABLE I. The extracted values of the parameters σ_i, E_i, and Γ_i, with $i = 1,2$, obtained by fitting the experimental data [18,19] for the photoabsorption and the photofission cross sections.

Nuclei	E_1 (MeV)	σ_1 (mb)	Γ_1 (MeV)	E_2 (MeV)	σ_2 (mb)	Γ_2 (MeV)
^{232}Th photoabsorption	11.16 ± 0.02	253.31 ± 4.27	3.69 ± 0.07	14.03 ± 0.02	332.05 ± 3.79	4.85 ± 0.06
^{232}Th photofission	10.82 ± 0.06	14.89 ± 1.02	1.55 ± 0.20	14.29 ± 0.04	38.69 ± 0.98	3.39 ± 0.17
^{238}U photoabsorption	11.04 ± 0.01	304.08 ± 1.91	2.44 ± 0.02	13.97 ± 0.01	384.50 ± 1.51	4.25 ± 0.02
^{238}U photofission	10.86 ± 0.03	50.95 ± 1.42	2.35 ± 0.10	14.26 ± 0.02	139.63 ± 1.20	4.32 ± 0.06
^{236}U photoabsorption	11.00 ± 0.05	349.76 ± 16.31	2.00 ± 0.16	14.00 ± 0.08	444.91 ± 13.43	4.00 ± 0.19
^{236}U photofission	10.82 ± 0.05	76.61 ± 3.95	2.12 ± 0.18	14.21 ± 0.05	233.51 ± 3.29	4.83 ± 0.13
^{235}U photoabsorption	11.00 ± 0.06	349.76 ± 35.52	1.07 ± 0.17	14.00 ± 0.07	445.12 ± 16.07	4.00 ± 0.23
^{235}U photofission	10.91 ± 0.06	95.58 ± 5.14	1.99 ± 0.19	13.88 ± 0.03	380.47 ± 3.66	4.21 ± 0.07
^{234}U photoabsorption	11.05 ± 0.03	210.99 ± 12.33	1.08 ± 0.14	13.13 ± 0.06	446.18 ± 7.20	6.06 ± 0.09
^{234}U photofission	11.08 ± 0.03	163.78 ± 3.47	2.82 ± 0.09	14.59 ± 0.02	348.76 ± 3.21	4.07 ± 0.07
^{233}U photoabsorption	11.05 ± 0.02	239.83 ± 5.52	1.82 ± 0.07	13.91 ± 0.03	437.35 ± 3.81	5.43 ± 0.06
^{233}U photofission	11.02 ± 0.07	142.70 ± 11.37	1.73 ± 0.23	13.86 ± 0.06	407.64 ± 8.37	4.09 ± 0.13
^{237}Np photoabsorption	11.03 ± 0.02	246.41 ± 4.36	2.80 ± 0.06	14.14 ± 0.02	392.21 ± 2.42	5.17 ± 0.07
^{237}Np photofission	10.92 ± 0.01	158.44 ± 0.70	2.56 ± 0.02	14.35 ± 0.01	261.39 ± 0.54	4.10 ± 0.02
^{239}Pu photoabsorption	11.14 ± 0.03	310.12 ± 12.48	2.26 ± 0.12	13.53 ± 0.07	376.37 ± 10.08	4.72 ± 0.09
^{239}Pu photofission	11.30 ± 0.04	207.50 ± 5.49	2.72 ± 0.09	14.33 ± 0.03	311.29 ± 4.49	3.77 ± 0.09

nuclei [14,15], corresponding to the absorption of photons, which induce oscillations of the neutron and proton fluids in the nucleus against each other, and the superposition of two such lines for statically deformed spheroidal nuclei [16,17], corresponding to oscillations along each of the nondegenerate axes of the spheroid. The lower-energy line corresponds to oscillations along the longer axis and the higher-energy line along the shorter, since the absorption frequency decreases with increasing nuclear dimensions. Therefore, the semiclassical theory of the interaction between photons and nuclei entails that the shape of a fundamental resonance in the absorption cross section is given by [15,17]

$$\sigma_a^{\mathrm{GDR}}(E_\gamma) = \Sigma_{i=1}^{2} \frac{\sigma_i}{1 + \left[\frac{(E_\gamma^2 - E_i^2)}{E_\gamma \Gamma_i}\right]^2}, \qquad (1)$$

where σ_i, E_i, and Γ_i are the peak cross section, resonance energy, and full width at half maximum, respectively. We find that, like the photoabsorption cross sections, the photofission cross sections can also be described quite well by Eq. (1). The list of parameters σ_i, E_i and Γ_i for $i = 1,2$ extracted by fitting experimental data [18,19] are provided in Table I for both photoabsorption as well as photofission cross sections. It may be observed from Table I that for photoabsorption and photofission cross sections there are little changes in parameters E_i and Γ_i while σ_i decides the difference. Therefore, we find by fitting data of all the eight actinide nuclei that ratios $R_1 = \frac{(\sigma_1)_f}{(\sigma_1)_a}$ and $R_2 = \frac{(\sigma_2)_f}{(\sigma_2)_a}$ for γ absorption and subsequent fission scale as $c_1\zeta_f^2$ and $c_2\zeta_f^2$ respectively with $c_1 = 0.9978$, $c_2 = 1.4775$ where ζ_f [20] is given by

$$\zeta_f = 10.9 - 0.319Z^2/A \qquad (2)$$

with Z,A being the charge and mass numbers of the target nucleus implying $R_{i=1,2}$ depends quadratically as $a_{2i}f^2 + a_{1i}f + a_{0i}$ on the fissility $f = Z^2/A$. In Fig. 1, the measured photoabsorption and photofission cross sections (full circles) for ^{238}U as functions of incident photon energy are compared with the predictions (solid lines) of the hydrodynamic theory of photonuclear reactions for the giant dipole resonance region

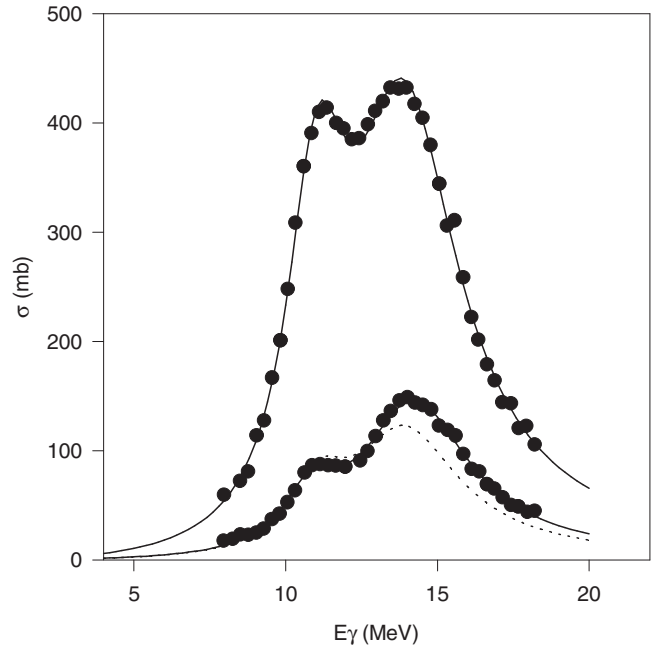

FIG. 1. Comparison of the measured photoabsorption and photofission cross sections (full circles) [18] for ^{238}U as functions of incident photon energy with predictions (solid lines) of the hydrodynamic theory of photonuclear reactions for the giant dipole resonance region that consists of Lorentz line shapes for spherical nuclei. The dotted line represents photofission cross sections obtained by using the ratio method.

that consists of Lorentz line shapes for spherical nuclei. The dotted line represents photofission cross sections obtained by using ratio method described above. It is apparent from Fig. 1 that the Lorentz line shape fitting is quite accurate, which reflects the fact that the uncertainties in the parameters listed in Table I are quite small. The ratio method predictions for photofission are almost as good up to the first GDR peak, whereas it is off by about 10% near the second GDR peak, but still provides much better predictions than that by the evaporation-fission process of the compound nucleus, which overestimates [21] the photofission cross sections at these energies.

III. MASS YIELD DISTRIBUTION OF PHOTOFISSION PRODUCTS

In the multimode-fission model, the mass distribution is interpreted as a sum of the contributions from the symmetric and asymmetric fission modes. Each fission mode corresponds to the passage through the fission barrier of specific shape. For each fission mode, the yield is described in the form of a Gaussian function. However, it is impossible to approximate the shape of the mass distributions by using only three Gaussian functions (two fission modes). For this, one needs five Gaussian functions (three fission modes). For ^{238}U fission, the symmetric fission mode (SM) is associated with $A = 117$ and for the asymmetric fission modes (ASMI, ASMII) in addition to broad maxima at $A = 138$ and $A = 96$, the mass distribution exhibits narrower maxima in mass-number regions around $A = 133$ and $A = 101$. Thus the total yield of fragments whose mass number is A is given by the expression

$$\begin{aligned} Y(A) &= Y_{\mathrm{SM}}(A) + Y_{\mathrm{ASMI}}(A) + Y_{\mathrm{ASMII}}(A) \\ &= C_{\mathrm{SM}} \exp\left[-\frac{(A - A_{\mathrm{SM}})^2}{2\sigma_{\mathrm{SM}}^2} \right] \\ &\quad + C_{\mathrm{ASMI}} \exp\left[-\frac{(A - A_{\mathrm{SM}} - D_{\mathrm{ASMI}})^2}{2\sigma_{\mathrm{ASMI}}^2} \right] \\ &\quad + C_{\mathrm{ASMI}} \exp\left[-\frac{(A - A_{\mathrm{SM}} + D_{\mathrm{ASMI}})^2}{2\sigma_{\mathrm{ASMI}}^2} \right] \\ &\quad + C_{\mathrm{ASMII}} \exp\left[-\frac{(A - A_{\mathrm{SM}} - D_{\mathrm{ASMII}})^2}{2\sigma_{\mathrm{ASMII}}^2} \right] \\ &\quad + C_{\mathrm{ASMII}} \exp\left[-\frac{(A - A_{\mathrm{SM}} + D_{\mathrm{ASMII}})^2}{2\sigma_{\mathrm{ASMII}}^2} \right]. \end{aligned} \tag{3}$$

In Fig. 2, approximation by the above five Gaussian functions for the mass distribution $Y(A)$ of fragments per 100 fission events originating from ^{238}U photofission induced by bremsstrahlung photons which corresponds to mean photon energy of 13.7 ± 0.3 MeV (that coincides with GDR peak for ^{238}U photofission) is plotted and compared with experimental data [13]. The various coefficients of Eq. (3) are obtained using the least square fitting method in the present calculation. The values of A_{SM}, D_{ASMI}, and D_{ASMII} are 117, 21, and 16, respectively, whereas the other parameter values are $C_{\mathrm{SM}} = 0.4929 \pm 0.2494$,

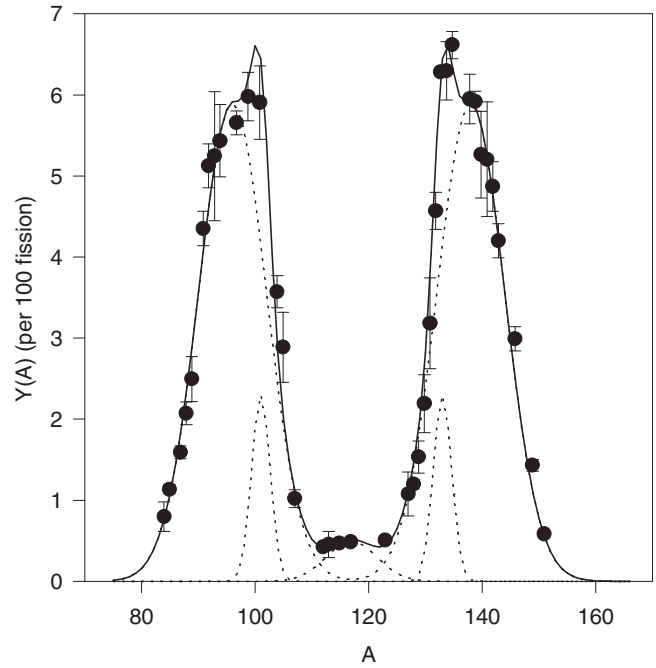

FIG. 2. Comparison of the measured mass yield distribution (full circles) for ^{238}U photofission induced by bremsstrahlung photons having mean photon energy of 13.7 MeV [13] with the prediction (solid line) of the five Gaussian formula for $Y(A)$. The dotted lines represent individual contributions of one symmetric Gaussian and two asymmetric double Gaussians.

$\sigma_{\mathrm{SM}} = 4.4732 \pm 3.3277$, $C_{\mathrm{ASMI}} = 5.8959 \pm 0.2765$, $\sigma_{\mathrm{ASMI}} = 5.9612 \pm 0.2824$, $C_{\mathrm{ASMII}} = 2.2945 \pm 0.2682$, and $\sigma_{\mathrm{ASMII}} = 1.6223 \pm 0.3901$. The errors in the fitted parameters are calculated from the correlation matrix in the final stage of the fitting procedure when changes in the fitted parameters by amounts equal to the corresponding uncertainties in the fitted parameters cause changes in the corresponding χ^2 by less than the stipulated value. Thus large uncertainty in a fitted parameter implies that the χ^2 hypersurface is rather flat with respect to that parameter. Obviously, the fact that the uncertainties in the parameters for the symmetric mode (single Gaussian) is large, while those for asymmetric modes (double Gaussians) are small, suggests that the importance of symmetric mode is somewhat less in determining the overall mass distribution.

IV. CHARGE DISTRIBUTION OF PHOTOFISSION PRODUCTS

The isobaric charge distribution of photofission products can be well simulated by a Gaussian function as

$$Y(A,Z) = \frac{Y(A)}{\sqrt{\pi C_p}} \exp\left[-\frac{(Z - Z_s + \Delta)^2}{C_p} \right], \tag{4}$$

where Z_s represents most stable isotope of fission fragment with mass number A while Δ measures the departure of the most probable isobar from the stable one. We deduce the expression for Z_s, theoretically, for the most stable nucleus by keeping mass number A constant while

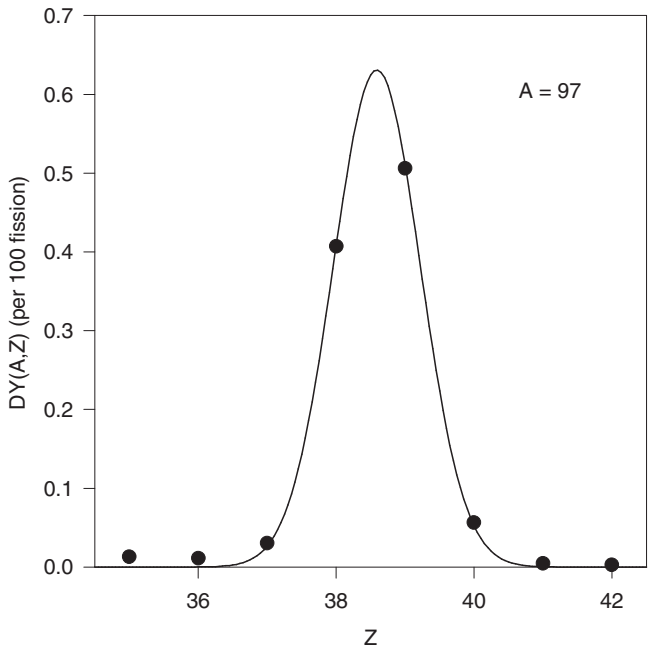

FIG. 3. Plot of fractional yield $DY(A,Z)$ as a function of charge number Z for fragment mass number $A = 97$ of ^{238}U photofission. Experimental data [13] are shown with full circles while the solid line represents the Gaussian charge distribution.

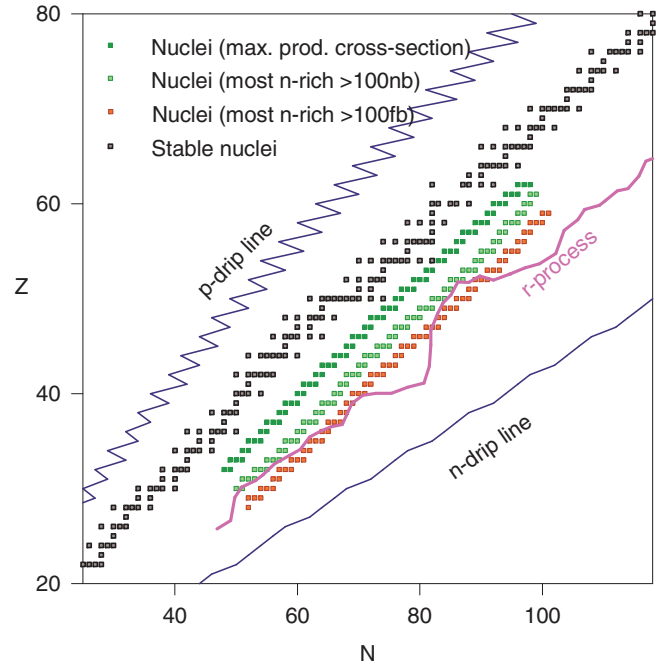

FIG. 4. (Color online) Plots of atomic number Z vs neutron number N for exotic nuclei produced by the photofission of ^{238}U by bremsstrahlung γs with mean photon energy of 13.7 MeV.

differentiating liquid drop model mass formula and setting the term $\partial M_{\text{nucleus}}(A,Z)/\partial Z\,|_A$ equal to zero as [22]

$$Z_s = \frac{[A + (a_c A^{2/3}/2x)]}{[(4a_{\text{sym}}/x) + (a_c A^{2/3}/x)]}, \tag{5}$$

where $x = 2a_{\text{sym}} + [(m_n - m_p)/2]$, a_c and a_{sym} are the Coulomb and symmetry energy coefficients, respectively, and m_p and m_n are the masses of proton and neutron respectively. The values of the parameter C_p which decides the dispersion and the shift parameter Δ for the most probable isotope are extracted by fitting experimental data [13] to be 0.8 and 3.8, respectively. The fractional yield $DY(A,Z)$ is defined as the ratio of the independent yield of production of nuclei belonging to a specific mass and charge number, $Y(A,Z)$, to the total yield $Y(A)$ for the same mass number A, that is, $DY(A,Z) = Y(A,Z)/Y(A)$. In Fig. 3, fractional yield $DY(A,Z)$ as a function of charge number Z for a particular fragment mass number $A = 97$ of ^{238}U photofission is plotted.

V. CALCULATION AND RESULTS

The photofission cross sections σ_f^{GDR} are calculated using Lorentz line shape in Eq. (1) for γ absorption while replacing σ_i by the ratio method described in Sec. II. The production cross sections of individual fragments for ^{238}U photofission induced by bremsstrahlung photons are obtained by multiplying fission cross section by charge distribution, which means $\sigma_f(A,Z) = \sigma_f^{\text{GDR}}.Y(A,Z)/100$. The endpoint energy of 29.1 MeV (the energy of electrons which produce bremsstrahlung γs when stopped by a W converter) is so chosen because it corresponds to the mean γ energy of 13.7 ± 0.3 MeV that coincides with GDR peak for ^{238}U photofission. In Table II, the theoretical cross sections along with uncertainties (arising out of uncertainty in the excitation energy) for the most probable (produced with highest production cross section) isobars with corresponding neutron and proton numbers for the fission fragments are tabulated. Corresponding atomic numbers Z_s for the most stable nuclei are calculated using Eq. (5) with values for $a_c = 0.71$ MeV and $a_{\text{sym}} = 23.21$ MeV [22]. The proton and neutron drip lines are calculated theoretically from modified liquid drop model mass formula [23] using the logic [24] that the nucleus from which removal of a single neutron (and any more) makes the one proton separation energy negative defines a proton drip line nucleus, and likewise the nucleus to which addition of a single neutron (and any more) makes the one neutron separation energy negative defines a neutron drip line nucleus.

VI. PRODUCTION OF NEUTRON-RICH NUCLEI

Short-lived exotic nuclei play a crucial role in heavy element synthesis and the evolution of stars. The rapid neutron capture process (r-process) produces neutron-rich nuclei. The predicted r-process reaction path has mostly been inaccessible experimentally. Using RIB one hopes to study this region in detail. A key question is whether the unusual properties of exotic nuclei alter the r-process reaction rates and path. It is, therefore, important to estimate the production cross sections of n-rich nuclei produced through ^{238}U photofission and investigate how many nuclei in the r-process path can reached in the laboratory.

In Fig. 4, atomic number Z versus neutron number N are plotted for exotic nuclei produced by the photofission of ^{238}U with mean photon energy of 13.7 ± 0.3 MeV. The

TABLE II. The theoretical cross sections for most probable (produced with highest production cross section) isobars with corresponding neutron and proton numbers for the fission fragments.

A	N	Z	Z_s	σ (mb)
80	48	32	36	0.116 ± .002
81	49	32	36	0.186 ± .003
82	49	33	36	0.230 ± .003
83	50	33	37	0.423 ± .006
84	51	33	37	0.502 ± .008
85	51	34	38	0.786 ± .012
86	52	34	38	1.069 ± .016
87	52	35	38	1.187 ± .018
88	53	35	39	1.856 ± .028
89	54	35	39	1.882 ± .029
90	54	36	40	2.615 ± .040
91	55	36	40	3.057 ± .047
92	55	37	40	2.982 ± .045
93	56	37	41	4.023 ± .061
94	57	37	41	3.545 ± .054
95	57	38	42	4.274 ± .065
96	58	38	42	4.375 ± .067
97	58	39	42	3.714 ± .057
98	59	39	43	4.637 ± .071
99	60	39	43	4.050 ± .062
100	60	40	44	4.804 ± .073
101	61	40	44	4.813 ± .073
102	61	41	44	3.328 ± .051
103	62	41	45	3.118 ± .047
104	63	41	45	1.874 ± .029
105	63	42	46	1.431 ± .022
106	64	42	46	1.127 ± .017
107	64	43	46	0.651 ± .010
108	65	43	47	0.647 ± .010
109	66	43	47	0.446 ± .007
110	66	44	48	0.357 ± .005
111	67	44	48	0.345 ± .005
112	68	44	48	0.250 ± .004
113	68	45	49	0.326 ± .005
114	69	45	49	0.329 ± .005
115	69	46	49	0.317 ± .005
116	70	46	50	0.394 ± .006
117	71	46	50	0.328 ± .005
118	71	47	51	0.371 ± .006
119	72	47	51	0.364 ± .006
120	72	48	51	0.275 ± .004
121	73	48	52	0.333 ± .005
122	74	48	52	0.291 ± .004
123	74	49	53	0.310 ± .005
124	75	49	53	0.399 ± .006
125	76	49	53	0.385 ± .006
126	76	50	54	0.632 ± .010
127	77	50	54	0.815 ± .012
128	77	51	54	0.942 ± .014
129	78	51	55	1.555 ± .024
130	79	51	55	1.865 ± .028
131	79	52	56	2.858 ± .043
132	80	52	56	4.160 ± .063
133	81	52	56	3.715 ± .057
134	81	53	57	4.995 ± .076
135	82	53	57	4.524 ± .069
136	82	54	57	3.844 ± .058
137	83	54	58	4.587 ± .070
138	84	54	58	3.893 ± .059
139	84	55	59	4.124 ± .063
140	85	55	59	4.255 ± .065
141	86	55	59	3.017 ± .046
142	86	56	60	3.547 ± .054
143	87	56	60	3.018 ± .046
144	87	57	60	2.240 ± .034
145	88	57	61	2.288 ± .035
146	89	57	61	1.613 ± .025
147	89	58	62	1.310 ± .020
148	90	58	62	1.111 ± .017
149	91	58	62	0.652 ± .010
150	91	59	63	0.576 ± .009
151	92	59	63	0.407 ± .006
152	92	60	63	0.224 ± .003
153	93	60	64	0.191 ± .003
154	94	60	64	0.113 ± .002
155	94	61	64	0.067 ± .001
156	95	61	65	0.048 ± .001
157	96	61	65	0.024 ± .000
158	96	62	66	0.015 ± .000
159	97	62	66	0.009 ± .000
160	98	62	66	0.004 ± .000
161	98	63	67	0.003 ± .000

results of three sets of calculations are presented which correspond to (i) nuclei with largest cross sections, that is, most probable isobars with corresponding neutron and proton numbers for the fission fragments, (ii) the most neutron-rich isobars subject to production cross sections >100 nb, and (iii) the most neutron-rich isobars subject to production cross sections >100 fb. The experimentally observed β stable nuclei as well as the theoretical proton and neutron drip lines along with the line of r-process nuclei are also shown in Fig. 4 in order to highlight how far one can march away from the line of β stability towards the neutron-rich nuclei using ^{238}U photofission. It is interesting to note here that the waiting point nuclei in the r-process path such as ^{80}Zn and ^{134}Sn are produced with cross sections 2.6 and 0.18 μb, respectively, while other nuclei in the r-process path such as ^{98}Kr and ^{110}Zr are produced with lesser cross sections of 6.7×10^{-2} μb and 1.6×10^{-5} μb, respectively. As expected, cross sections fall rapidly with increasing mass number because of the neutron richness, which is obvious from Eq. (4). Furthermore, as long as the A/Z ratio of photofission products remains same, the cross sections are found to be about the same (e.g., 1 μb for $A/Z = 2.66$), which is due to the fact that then $Z - Z_s$ remains the same.

It is worthwhile to mention here that at high energies [25] the projectile fragment separator RIB facilities, being developed in different laboratories, could also provide the scope for

producing many new exotic nuclei through fragmentation of high-energy radioactive ion beams [26,27].

VII. SUMMARY AND CONCLUSION

In summary, we find that, like the photoabsorption cross sections, the photofission cross sections can also be described quite well by Lorentz line shapes. The ratio method predictions using Eq. (2) for photofission are almost as good as the Lorentz line shape fitting, whereas the evaporation-fission process of the compound nucleus overestimates the photofission cross sections. We have performed a simultaneous analysis for the comparison of the behavior of the symmetric and asymmetric modes. The phenomenological methodology for obtaining independent and cumulative yields of isotopes produced in photofission is described. A detailed analysis of the production of each nuclear isobar via fission and the mass distributions of products originating from the photofission induced by bremsstrahlung photons is provided. The endpoint energy of 29.1 MeV, which is the energy of electrons that produce bremsstrahlung γs when stopped by a W converter, is so chosen as to correspond the mean γ energy of 13.7 ± 0.3 MeV, which coincides with GDR peak for ^{238}U photofission.

The present calculations indicate clearly that many of the r-process nuclei in intermediate mass range can be obtained in the laboratory with measurable cross sections by photofission. However, in the higher mass range, more than $A = 140$, one would need to go for nuclear processes other than photonuclear reactions to produce them.

[1] W. T. Diamond, Nucl. Instrum. Methods Phys. Res., Sect. A **432**, 471 (1999).
[2] F. Ames *et al.*, Conf. Proc. **C1205201**, 64 (2012) of the 3rd International Conference on Particle accelerator (IPAC 2012), New Orleans, USA, 2012.
[3] J. Richards *et al.*, Conf. Proc. ICALEPCS2011, Grenoble, France, 465 (2011).
[4] Yu. Ts. Oganessian *et al.*, Nucl. Phys. A **701**, 87 (2002).
[5] M. Cheikh Mhamed *et al.*, Nucl. Instrum. Methods Phys. Res., Sect. B **226**, 4092 (2008).
[6] A. Chakrabarti *et al.*, Nucl. Instrum. Methods Phys. Res., Sect. B **317**, 253 (2013).
[7] H. Naik, F. Carre, G. N. Kim, F. Laine, A. Sari, S. Normand, and A. Goswami, Eur. Phys. J. A **49**, 94 (2013).
[8] S. Essabaa *et al.*, Nucl. Instrum. Methods Phys. Res., Sect. B **204**, 780 (2003).
[9] U. Brosa, S. Grossmann, and A. Müller, Phys. Rep. **197**, 167 (1990).
[10] M. C. Duijvestijn, A. J. Koning, and F.-J. Hambsch, Phys. Rev. C **64**, 014607 (2001).
[11] N. A. Demekhina and G. S. Karapetyan, Phys. At. Nucl. **71**, 27 (2008).
[12] S. Pommé, E. Jacobs, K. Persyn *et al.*, Nucl. Phys. A **560**, 689 (1993).
[13] B. S. Ishkhanov and A. A. Kuznetsov, Phys. At. Nucl. **77**, 824 (2014).
[14] M. Goldhaber and E. Teller, Phys. Rev. **74**, 1046 (1948).
[15] H. Steinwedel and J. H. D. Jensen, Z. Naturforsch. A **5**, 413 (1950).
[16] K. Okamoto, Prog. Theor. Phys. (Kyoto) **15**, 75L (1956).
[17] M. Danos, Nucl. Phys. **5**, 23 (1958).
[18] A. Veyssiére *et al.*, Nucl. Phys. A **199**, 45 (1973).
[19] J. T. Caldwell, E. J. Dowdy, B. L. Berman, R. A. Alvarez, and P. Meyer, Phys. Rev. C **21**, 1215 (1980).
[20] R. Vandenbosch and G. T. Seaborg, Phys. Rev. **110**, 507 (1958).
[21] T. Mukhopadhyay and D. N. Basu, Eur. Phys. J. A **45**, 121 (2010).
[22] P. R. Chowdhury and D. N. Basu, Acta Phys. Pol. B **37**, 1833 (2006).
[23] C. Samanta and S. Adhikari, Phys. Rev. C **65**, 037301 (2002).
[24] D. N. Basu, Int. J. Mod. Phys. E **13**, 747 (2004).
[25] D. Bhowmick, A. Chakrabarti, D. N. Basu, P. Ghosh, and R. Goswami, Mod. Phys. Lett. A **13**, 2665 (1998).
[26] A. C. Mueller *et al.*, Nucl. Instrum. Methods Phys. Res., Sect. B **56**, 559 (1991)
[27] J. M. D'Auria, Nucl. Instrum. Methods Phys. Res., Sect. B **99**, 330 (1995).